Article

A Copper Nanocluster-Based Fluorescent Probe for Real-Time Imaging and Ratiometric Biosensing of Calcium Ion in Neurons

Zhichao Liu, Xia Jin, Sanjun Zhang, and Yang Tian

Anal. Chem., **Just Accepted Manuscript** • DOI: 10.1021/acs.analchem.8b05360 • Publication Date (Web): 08 Jan 2019

A Copper Nanocluster-Based Fluorescent Probe for Real-Time Imaging and Ratiometric Biosensing of Calcium Ion in Neurons

Zhichao Liu,[†] Xia Jin,[†] Sanjun Zhang,[‡] and Yang Tian*[, †, ‡]

[†]Shanghai Key Laboratory of Green Chemistry and Chemical Processes, School of Chemistry and Molecular Engineering, East China Normal University, Dongchuan Road 500, Shanghai 200241, P. R. China

[‡]State Key Laboratory of Precision Spectroscopy, East China Normal University, North Zhongshan Road 3663, Shanghai 200062, P. R. China

ABSTRACT: Fluorescent calcium ions (Ca^{2+}) sensing and imaging have become an essential technique for investigation of signaling pathways of $Ca^{2+}$and understanding the role of Ca^{2+} in neurodegenerative disease. Herein, a copper nanoclusters (CuNCs)-based ratiometric fluorescent probe was developed for real-time sensing and imaging of Ca^{2+} in neurons, in which a specific Ca^{2+} ligand with two formaldehyde groups was synthesized and further conjugated with polyethyleneimine (PEI) to form a new ligand molecular for synthesis of CuNCs. Meanwhile, water-soluble Alex Fluor 660 NHS ester was immobilized onto CuNCs as a reference element. The developed ratiometric fluorescence nanoprobe demonstrated a good linearity with Ca^{2+} concentration in the range of 2-350 μM, and the detection limit was as achieved down to 220±11 nM. In addition, the response time of the present probe for Ca^{2+} was found to less than 2 s with good stability and high selectivity. Taking advantages of the developed nanoprobe including low cytotoxicity and good biocompatibility, it was discovered that histamine-induced cytoplasmic Ca^{2+} increase in various parts of neurons was different. Moreover, it was found $O_2^{\bullet-}$ induced cytoplasmic Ca^{2+} burst and $O_2^{\bullet-}$-induced neuronal death was possibly resulted from Ca^{2+} overload in neurons.

Calcium ion (Ca^{2+}) as a significant intracellular signaling molecule plays an indispensable role in signal transduction,[1] memory formation,[2] synaptic activity,[3] gene transcription,[1] and oxidative stress process[4]. More importantly, dysregulation of intracellular Ca^{2+} signaling has been implicated in the pathogenesis of Alzheimer's disease.[5] Since the changes in cytosolic Ca^{2+} concentration are transitory, it is important to track the dynamic changes of intracellular Ca^{2+} concentration and understand the Ca^{2+} signal pathways in cells.

Fluorescence-based biosensors have attracted great interests because they are simple and effective for cellular native species sensing and imaging.[6-10] Several elegant fluorescent Ca^{2+} probes have been developed, such as genetically encoded fluorescent proteins (GFP)[11-13] , small organic molecule probes[14-17], and upconversion nanoparticle-based probes[18,19]. Our group is very interested in development of analytical methods for biosensing and imaging of metal ions and reactive oxygen species (ROS) in live brains, tissues, and cells. We have developed several inorganic-organic ratiometric fluorescent probes for determination of Cu^{2+}, Fe^{2+}, pH and other oxidative stress-related ROS in living cells and tissues.[20-25] However, it is still a challenging work to develop a fluorescent Ca^{2+} probe with high accuracy and selectivity, as well as good biocompatibility and long-term stability for fulfilling the requirements for selective imaging and accurate biosensing of Ca^{2+} in live cells. In fact, inorganic-organic composited probe may solve these problems well, because the designed organic molecules provide specific recognition for Ca^{2+} while fluorescent inorganic nanomaterials, like metal nanoclusters and carbon dots, demonstrate low cytotoxicity and long-term fluorescence stability.[26,27] Moreover, inner-reference molecules can also be conjugated onto the surface of nanomaterials to construct ratiometric probes with built-in correction, which shows high accuracy, independence of probe concentrations, fluctuation of excitation light intensity or environmental effects in complex samples.[6,28,29] Therefore, it is greatly desirable to develop an inorganic-organic ratiometric fluorescent probe for Ca^{2+} with high selectivity, good compatibility and long-term stability.

In this work, a specific Ca^{2+} ligand (CaL) with two formaldehyde groups was synthesized (Scheme 1A). Then, CaL was further attached onto polyethyleneimine (PEI) to develop a new template molecule (PEI-CaL) by Schiff base reaction between -CHO group of CaL and -NH_2 group of PEI. PEI-CaL plays as not only a specific recognition element for Ca^{2+}, but also a ligand for synthesis of copper nanoclusters (CuNCs). Then, CuNCs were synthesized using a template of PEI-CaL by reducing Cu^{2+} in the presence of ascorbic acid (AA). Next, the reference fluorescent molecule, Alexa Fluor 660 (AF660), was designed and conjugated onto the surface of as-prepared CuNCs to develop ratiometric fluorescent probe (CuNC@AF660) for accurate determination of Ca^{2+} (Scheme 1B). The developed CuNC@AF660 probe demonstrated two independent emission peaks emerged at ~590 nm and ~690 nm upon excitation at 488 nm, respectively. Compared with previous reported fluorescent Ca^{2+} probe, our developed ratiometric fluorescent CuNC@AF660 probe shows excellent water solubility due to the good water solubility of PEI-CaL. In addition, the developed CuNC@AF660 probe shows high selectivity owing to the presence of CaL. Moreover, our developed ratiometric fluorescent nanoprobe shows high accuracy by using AF660 as reference signal. The emission peak at 590 nm increased with increasing concentration of Ca^{2+} while the fluorescence intensity

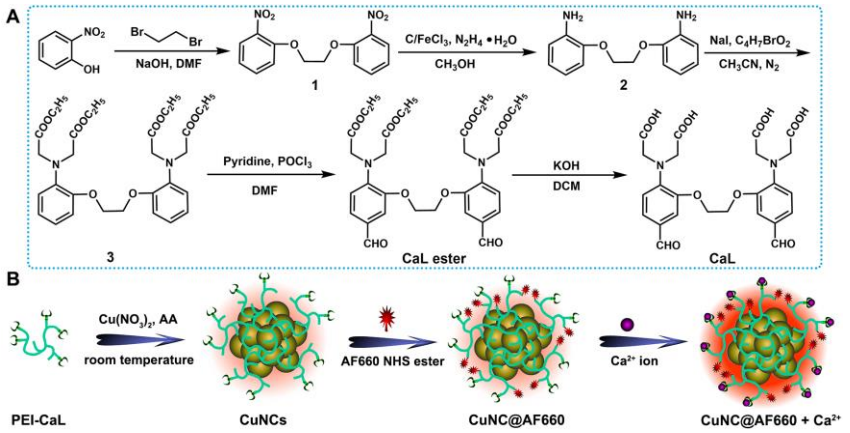

Scheme 1. (A) Synthesis routes of CaL and CaL ester. (B) Schematic illustration of working principle of CuNC@AF660 ratiometric fluorescent probe for Ca^{2+} sensing.

at 690 nm kept unchanged, resulting in ratiometric determination of Ca^{2+} with high accuracy. The present ratiometric fluorescent probe showed high selectivity against other metal ions, amino acids, calcium-containing proteins and common ROS, as well as long-term stability. In addition, taking advantages of CuNC@AF660 probe including low cytotoxicity, good biocompatibility and rapid response dynamics, the developed fluorescent probe for Ca^{2+} was successfully applied in biosensing and imaging of Ca^{2+} in neurons. Using this useful probe, it was found that histamine-induced cytoplasmic Ca^{2+} increase in various parts of neurons was different. Furthermore, we can see that $O_2^{\bullet-}$ induced cytoplasmic Ca^{2+} burst and $O_2^{\bullet-}$-induced neuronal death was possibly resulted from Ca^{2+} overload in neurons.

EXPERIMENTAL SECTION

Reagents and Chemicals. 2-nitrophenol, 1,2-dibromoethane, carbon powder (C), ethylbromoacetate ($C_4H_7BrO_2$), dimethyl formamide (DMF) and 3-(4,5-dimethyl-2-thiazolyl)-2,5-diphenyl-2-H-tetrazolium bromide (MTT) were purchased from Aladdin Chemistry Co. Ltd. (Shanghai, China). Ferric trichloride ($FeCl_3$), n-hexane, acetonitrile, methanol (CH_3OH), ethyl alcohol (EtOH), hydrazine hydrate ($N_2H_4 \bullet H_2O$), sodium iodide (NaI), methylbenzene, anhydrous sodium sulfate (Na_2SO_4), phosphorus oxychloride ($POCl_3$), sodium hydroxide (NaOH) and sodium bicarbonate ($NaHCO_3$) were provided by Sinopharm Chemical Reagent Co. Ltd. (Shanghai, China). Alexa Fluor 660 NHS ester and Hank's balanced salt solution (HBSS, no calcium, no magnesium, no phenol red) was purchased from Thermo Fisher Scientific (U.S.A). All chemicals were of analytical grade were used without further purification and modification. All samples were prepared by deionized water purified by Milli-Q water purification system.

Instruments and Methods. Nuclear magnetic resonance (NMR) spectra were recorded on a Bruker 500 MHz spectrometer (Bruker, Germany). Mass spectra (MS) were recorded by Agilent 6890 (Agilent, U.S.A). The fluorescence spectra and UV-vis absorption spectra were obtained with a Hitachi F-4500 fluorescence spectrophotometer and Hitachi UH5300 spectrophotometer (Hitachi, Japan). Fourier transform infrared spectroscopy (FTIR) spectra were obtained using a Thermo Scientific Fourier Transform Infrared spectrometer at resolution of 4 cm^{-1} in the range of 500 - 4000 cm^{-1} (Thermo Fisher Scientific, U.S.A). Atomic force microscope (AFM) images were recorded in the ScanAsyst mode under ambient conditions (Bruker, Germany). Transmission electron microscope (TEM) images were collected with a JEM-2100F transmission electron microscope (JEOL, Japan). The apoptosis assay was conducted at a FACS Calibur flow cytometry (Becton, Dickinson and Company, U.S.A). The absorbance of cytotoxicity was recorded by a Varioskan LUX multimode microplate reader (Thermo Fisher Scientific, U.S.A). Fluorescence confocal imaging was performed with a Leica TCS-SP8 confocal scanning microscope using a 63× oil objective and a numerical aperture of 1.40 (Leica, Germany).

Synthesize of Ca^{2+} ligand (CaL). The synthetic route for CaL was described in Scheme 1A, according to literatures with some modification.[30]

Compound 1: A mixture of NaOH (4.8 g, 12 mmol), H_2O (4.5 mL) and 2-nitrophenol (15.30 g, 11 mmol) in 30 mL DMF was heated to 60 °C for 30 min with stirring. Then 1, 2-dibromoethane (5.1 mL) was added and heated to 130 °C for 3 h. After cooling down to room temperature, the mixture was diluted to 100 mL with water and filtered. The precipitate was washed with 10% $NaHCO_3$ and water (w/w) for at least three times. Recrystallization from ethanol yielded 1.17 g compound 1. Yield: 70%. ^{1}H NMR (DMSO, 500 MHz), δ: 7.85 (d, 2H, J=8.1), 7.65 (t, 2H, J=8.0), 7.43 (d, 2H, J=8.5), 7.14 (t, 2H, J=7.8), 4.54 (s, 4H).

Compound 2: A mixture of compound 1 (4.56 g, 15 mmol), carbon powder (0.24 g, 20 mmol) and $FeCl_3$ (0.032 g, 0.2 mmol) was heated to 80 °C in 90% methanol (w/w, 45 g) under N_2 atmosphere. Then, 85% $N_2H_4 \bullet H_2O$ (3 mL) was added dropwise within 20 min. The mixture was refluxed for 5 h. It was filtered while hot and washed with hot methanol. The combined filtrate was evaporated and recrystallized from ethanol to give 2.20 g faint yellow crystals. Yield: 60%. ^{1}H NMR (DMSO, 500 MHz), δ: 6.87 (dd, 2H, J=8.0), 6.71 (td, 2H, J=7.4), 6.66 (dd, 2H, J=7.8), 6.53 (td, 2H, J=7.6), 4.66 (s, 4H), 4.28 (s, 4H).

Compound 3: A mixture of compound 2 (1.54 g, 6.32 mmol), NaI (0.38 g, 2.53 mmol), K_2HPO_4 (7.212 g, 31.6 mmol) and ethyl bromoacetate (4 mL, 36.4 mmol) in 25 mL anhydrous acetonitrile was refluxed under nitrogen for 18 h. Toluene was added after distilling the solvent. The solution was washed with water and saturated brine. Organic layer was dried over Na_2SO_4 and evaporated. Recrystallization from ethanol gave 2.23 g product as white powder. Yield: 60%. ^{1}H NMR (DMSO, 500 MHz), δ: 6.99-6.91 (m, 2H), 6.86 (tt, 4H, J=7.4), 6.77-6.65 (m, 2H), 4.21 (s, 4H), 4.10 (s, 8H), 3.97 (m, 8H, J=7.1), 1.08 (t, 12H, J=7.2).

CaL ester: A mixture compound 3 (0.882 g, 1.5 mmol) and 150 μL pyridine was dissolved in 3 mL DMF. Then, 1.2 mL $POCl_3$ was dropped slowly at 0 °C. The reaction mixture was stirred at room temperature for 30 min and heated to 60 °C for 1 h and then back to room temperature for 20 h. The mixture was poured into aqueous NaOH mixed with ice. The aqueous layer was extracted with CH_2Cl_2 for three times. The combined organic layer was washed with water and saturated brine for three times. After drying with Na_2SO_4 and evaporation, the residue was chromatographed on silica in petroleum ether: ethyl acetate = 4:1 (v/v) to yield 193 mg CaL ester. Yield: 20%. ^{1}H NMR (DMSO, 500 MHz), δ: 9.78 (s, 2H), 7.45 (dd, 2H, J=8.3), 7.38 (d, 2H, J=1.8), 6.73 (d, 2H, J=8.3), 4.23 (d, 12H, J=10.4), 3.97 (q, 8H, J=7.1), 1.05 (t, 12H, J=7.1). ^{13}C NMR (DMSO, 500 MHz): δ = 191.10, 170.70, 149.00, 144.98, 129.19, 126.12, 116.37, 111.62, 67.44, 60.89, 53.92, 14.22 ppm.

CaL: CaL ester (130 mg, 0.2 mmol) was added into 3 mL KOH solution (1 M, dissolved in EtOH), then 1 mL CH_2Cl_2 was added. The mixture was stirred at 37°C for 24 h. After that, the mixture was adjusted to a pH range of 4-5 by HCl. The solid was filtered and product was extracted with abundant CH_2Cl_2. After drying with Na_2SO_4 and evaporation, 65 mg CaL ester was obtained. Yield: 60%. ^{1}H NMR (DMSO, 500 MHz), δ: 12.56 (s, 4H), 9.75 (s, 2H), 7.44 (dd, 2H, J=8.4), 7.38 (d, 2H, J=1.8), 6.71 (d, 2H, J=8.4), 4.30 (s, 4H), 4.16 (s, 8H). ^{13}C NMR (DMSO, 500 MHz): δ = 191.00, 172.37, 148.75, 145.41, 128.78, 126.13, 116.07, 112.88, 67.49, 54.39 ppm.

Preparation of CuNCs and CuNC@AF660. In order to synthesize CuNCs, PEI-CaL was first prepared by the reaction between PEI and CaL. In brief, 1 mL PEI (5 mM, WM: 1800) was dissolved in ethanol, then 1 mL CaL solution (30 mM, dissolved in CH_2Cl_2) was added, the mixture was reacted at room temperature for 12 h. PEI-CaL was obtained by removing CH_2Cl_2 through reduction vaporization and unreacted CaL was removed by dialysis. Next, PEI-CaL solution was adjusted to pH 5 by acetic acid, then 3 mL $Cu(NO_3)_2$ solution (1 mM) was added under stirring. After 10 min, 10 mg ascorbic acid was added and reacted for another 8 h. The obtained CuNCs capped with PEI-CaL were purified by ultrafiltration with a Millipore (30 K, molecular weight cutoffs) with 16000 rpm for 10 min and stored at 4 °C for further using. For preparing the ratiometric fluorescence probe (CuNC@AF660), the obtained CuNCs (1 mL) were mixed with appropriate volume of AF660 NHS ester solution in PBS buffer (pH 7.4), and reacted at room temperature under stirring overnight. Finally, CuNC@AF660 was purified by ultrafiltration.

Calculation of the mass concentrations of CuNCs and CuNC@AF660. In order to determine the concentration of CuNCs, three pre-weighed tubes (m_0) were added with 0.5 mL of CuNCs, respectively. Then, the tubes were dried to evaporate water. Finally, the tubes containing dry CuNCs were weighed again (m_1). The mass concentration of CuNCs was calculated by dividing the difference in masses (m_1-m_0) by 0.5 mL and taking the average. The mass concentration of CuNC@AF660 was obtained by the same method with that of CuNCs.

Primary culture of mouse cortical neurons. The experimental protocols were approved by Animal Care and Use Committee of East China Normal University, Shanghai, China. Primary cultures of mouse cortical neurons were prepared as described previously.[23] Briefly, postnatal day 1 C57BL/6 wild-type mice were anesthetized with halothane. Brains were removed rapidly and placed in ice-cold Ca^{2+} and Mg^{2+} free phosphate-buffered saline (PBS). Tissues were dissected and incubated with Papain for 15 min at 37 °C, followed by trituration with fire-polished glass pipettes, and plated in poly-D-lysine-coated 35-mm Petri dishes with 20 mm bottom wells at a density of 1×10^6 cells per dish. Neurons were cultured with Neurobasal medium supplemented with B27 and L-Glutamin, then maintained at 37 °C in a humidified 5% CO_2 atmosphere incubator. Cultures were fed twice a week and used for all the assays 8-14 days after plating.

Cytotoxicity and apoptosis assay. For cytotoxicity assay, different concentrations of CuNC@AF660 probe were added into pre-incubated neurons in 96-well plates and cultured for 24 and 48 h, respectively. Subsequently, 20 μL MTT were added to each well in dark. After reaction for 4 h, the mixed solution was removed and 80 μL DMSO was added. After shaking for 5 min, the absorbance was measured at 490 nm. Cell viability values were determined according to the following formulae: cell viability (%) = absorbance of the experimental group/ absorbance of the blank control group × 100%. For apoptosis assay, different concentrations of CuNC@AF660 probe were cultured with pre-incubated neurons for 24 h. After removing the culture media, the cells were collected with the help of EDTA-free trypsin. After washing with HBSS, the cells were re-suspended in 300 μL binding buffer and incubated with 5 μL FITC-Annexin V and 5 μL propidium iodide solution for 30 min in dark. Apoptosis assay was detected at an excitation wavelength of 480 nm.

Fluorescence confocal imaging. For Ca^{2+} imaging, CuNC@AF660 probe (90 μg/mL) was cultured with neurons for 1 h in Hanks' balanced salt solution with no Ca^{2+} and Mg^{2+} (HBSS), then washed by HBSS for twice and different concentrations of Ca^{2+} with 5 μM calcimycin (a divalent cation ionophore which allows Ca^{2+} to cross the cell membrane) and cultured for another 30 min in HBSS, cell imaging was carried out after cells were washed with HBSS for twice. For histamine or $O_2^{\bullet-}$-stimulating imaging, CuNC@AF660 probe was first cultured with neurons for 1 h in HBSS, then the neurons were washed by HBSS for twice. After that, the neurons were cultured in neurobasal medium, histamine (50 μM) or $O_2^{\bullet-}$ (80 μM) was added and the images were obtained with time interval of 20 s.

RESULTS AND DISCUSSION

Preparation and characterization of CuNCs. In order to realize Ca^{2+} detection with high selectivity, a Ca^{2+} ligand (CaL) with two formaldehyde groups was first designed and synthesized. The structures of CaL and intermediates were confirmed by ^{1}H NMR (Figures S1-S5) and ^{13}C NMR (Figures S6, S7), and the molecular weights of CaL and CaL ester were characterized by mass spectroscopy (Figures S8, S9). Fourier transform infrared spectroscopy (FTIR) spectrum of CaL shows two distinct peaks at 2760 and 1740 cm^{-1}, assigned to the stretching vibration of C-H and C=O, respectively, indicating the presence of -CHO group in CaL (Figure 1A). Other characteristic groups of CaL can also be found from FTIR spectra (Figure S10). Then, CaL was further conjugated onto PEI to develop a new template molecule (PEI-CaL) by Schiff base reaction between -CHO group of CaL and -NH_2 group of PEI for synthesizing CuNCs. From FTIR spectrum, PEI shows two distinct peaks emerged at 1650 and 1311 cm^{-1}, which belongs to N-H stretching vibration and bending vibration of amino groups. After CaL was conjugated onto PEI to form PEI-CaL, a new peak at 1572 cm^{-1} was observed, which pertained to the stretching vibration of C=N,

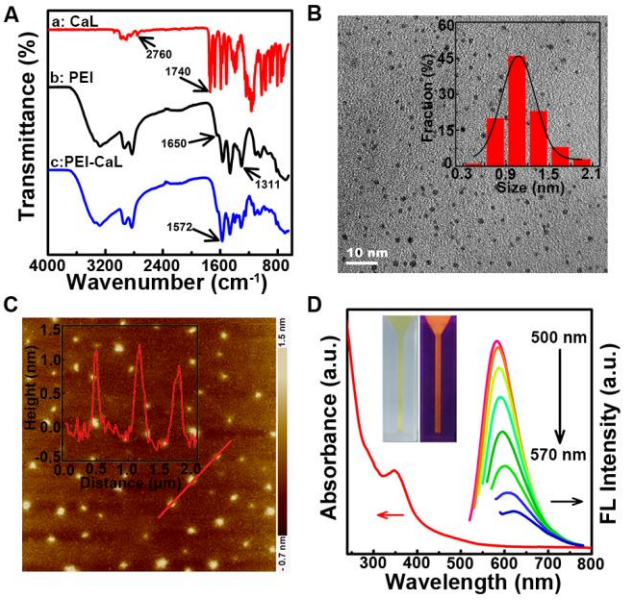

Figure 1. (A) FTIR spectra of CaL, PEI, and PEI-CaL. (B) TEM image of CuNCs. Inset shows diameter distributions of CuNCs. (C) AFM image of CuNCs deposited on freshly cleaved mica. Inset shows height distributions of CuNCs along the line shown in C. (D) UV-vis absorption spectrum and fluorescence spectra of CuNCs (90 μg/mL) at excitation wavelengths from 500 nm to 570 nm with interval of 10 nm. Insets show photographs of CuNCs solution (90 μg/mL) under ambient light (left) and illuminated by an UV lamp of 365 nm (right).

indicating PEI-CaL was successfully conjugated by forming Schiff base complexes.[31] Next, CuNCs were synthesized using a template of PEI-CaL. As shown in Figure 1B, transmission electron microscopy (TEM) image shows that CuNCs are monodispersed with averaging size about 1.1±0.4 nm (Insert in Figure 1B). The typical atomic force microscope (AFM) image of CuNCs demonstrates many dot-like compositions with cross-sectional heights of ~1 nm (Figure 1C). On the other hand, CuNCs display three well-resolved absorption peaks at 284, 350 and 476 nm as well as the bright jacinth fluorescent CuNCs (under a 365 nm UV lamb) exhibit excitation-dependent fluorescence emissions (Figure 1D and insert). In addition, the fluorescence intensity of CuNCs increased with the increasing concentration ratio of PEI-CaL to Cu^{2+}, and the fluorescence intensity reached stable when the concentration ratio of PEI-CaL to Cu^{2+} was 2:1 (Figure S11A). Furthermore, the fluorescence intensity of various batches of CuNCs was comparable (< 1%) (Figure S11B). Compared with previously reported CuNCs,[32] the optimal emission of our developed CuNCs red-shifted by ~70 nm. The fluorescence quantum yield (QY) of the developed CuNCs was ~20% by using fluorescein as a reference chromophore (Figure S12). In order to confirm the valence state of Cu in CuNCs, X-ray photoelectron spectroscopy (XPS) was employed to characterize the prepared CuNCs. XPS spectrum shows typical elements of C, N, O and Cu in CuNCs (Figure S13A). XPS spectrum of the developed CuNCs in Cu 2p region demonstrates two intense peaks at 932.2 and 952.0 eV (Figure S13B), assigned to the binding energies of $2p_{3/2}$ and $2p_{1/2}$ electrons of Cu (0). Meanwhile, no peak was observed at 942.0 eV, which belongs to binding energy of Cu (II) electrons.[33] It is of great importance to mention that $2p_{3/2}$ binding energy of Cu (0) is only ~0.1 eV away from that of Cu (I). Therefore, the valence state of the obtained CuNCs most likely lies between 0 and +1. The results demonstrated that the synthesized CuNCs through PEI-CaL template were stable against oxidation in air.

In addition, considering the high salt concentrations in cells, the fluorescence of CuNCs exposed to different concentrations of NaCl were also checked. The fluorescence intensity of the present CuNCs showed no obvious change even in 1 M of NaCl (< 4.1%) (Figure S14A). Moreover, different thiol compounds and phosphate had no apparent influence on the fluorescence of CuNCs (< 3.5%) (Figure S14B). All these results suggest good stability of our developed CuNCs.

Synthesis and characterization of CuNC@AF660 probe for Ca^{2+} biosensing. For improving the accuracy of Ca^{2+} biosensing in live cells, Alexa Fluor 660 (AF660) was then attached onto CuNCs to develop CuNC@AF660 ratiometric fluorescent probe. FTIR spectra were used to characterize the assembly of CuNC@AF660. Individual FTIR spectrum of CuNCs shows one board peak emerged at 3374 cm^{-1} and one narrow peak around 1643 cm^{-1} (Figure 2A), which belong to the stretching vibrations of N-H. In addition, a peak located at 1400 cm^{-1} was also observed, which attributes to the bending vibration of N-H, promising the presence of amino group on CuNCs. On the other hand, AF660 NHS ester shows a distinct peak at 1663 cm^{-1}, which pertains to the stretching vibration of C=O from amide I band, demonstrating the presence of carboxylic NHS ester in AF660 NHS ester. However, after AF660 NHS ester was conjugated onto CuNCs to form CuNC@AF660, the stretching vibration of C=O from amide I band blue-shifted to 1653 cm^{-1}. Furthermore, a new peak located at 1566 cm^{-1} was observed, which belongs to the bending vibration of N-H from amide II band, confirming the successful attachment of AF660 NHS ester onto CuNCs by forming amide bond. In addition, dynamic light scattering (DLS) results showed that the average diameter of individual CuNCs was estimated to 98±12 nm (Figure S15). However, after the AF660 was conjugated onto CuNCs to form CuNC@AF660 probe, the average diameter of CuNC@AF660 probes increased to 110±10 nm. The results further prove that AF660 was successfully conjugated onto CuNCs. Moreover, CuNC@AF660 display two emissions at ~590 nm and ~690 nm upon excitation at 488 nm, respectively, ascribed to that of CuNCs and AF660 NHS ester (Figure 2B).

Next, the stability of developed CuNC@AF660 probe was investigated. The fluorescence ratio of CuNC@AF660 probe ($F_{510\text{-}650}/F_{660\text{-}780}$) shows no obvious change even after the probe was incubated with different solutions for 5 h (< 1%) (Figure S16), indicating the high stability of developed CuNC@AF660 probe. It should be pointed out that cell imaging experiments were conducted within 2 h, thus the detection time is long enough for cell imaging. Meanwhile, the influence of concentration ratio of CuNCs to AF660 on the Ca^{2+} sensing was also investigated. The fluorescence enhancement efficiency (R) of CuNC@AF660 was obtained after 300 μM Ca^{2+} was added into the solution of CuNC@AF660 probe at different concentration ratio of CuNCs to AF660. The value of R increased with the increasing concentration ratio of CuNCs to AF660, and the R value reached stable when the concentration ratio of CuNCs to AF660 was 15:1 (Figure S17A). Moreover, no obvious difference (< 1%) was observed for the fluorescence intensity ratio ($F_{510\text{-}650}/F_{660\text{-}780}$) of various batches of CuNC@AF660 probes (Figure S17B). Furthermore, the effect of pH on the ratiometric fluorescent response of CuNC@AF660 to Ca^{2+} was also investigated. R value of CuNC@AF660 probe increased 5.04% when pH increased from 5.0 to 7.0 after addition of 250 μM Ca^{2+} into CuNC@AF660 solution (Figure S18). Meanwhile, R value of

CuNC@AF660 probe decreased 4.04% when pH changes from 7.0 to 9.0 after addition of 250 μM Ca^{2+} into CuNC@AF660 solution. Thus, pH between 5.0-9.0 had no obvious influence on ratiometric fluorescent response of CuNC@AF660 to Ca^{2+}. The results proved that the developed CuNC@AF660 probe can be used in Ca^{2+} sensing and imaging in cytoplasm.

In order to confirm the working principle, ratiometric fluorescent probe was further used to detect Ca^{2+} in cell lysis buffer. As shown in Figure 2C, with increasing concentration of Ca^{2+}, the fluorescent intensity of CuNCs ($F_{510\text{-}650}$: 510-650 nm) increased apparently while the fluorescence intensity of AF660 ($F_{660\text{-}780}$: 660-780 nm) kept no obvious change. Thus, the fluorescence from AF660 provided an inner reference for built-in correction, which may eliminate the environmental interference for determination of Ca^{2+}. In consequence, the fluorescent signal ratio ($F_{510\text{-}650}/F_{660\text{-}780}$) gradually enhanced with increasing concentration of Ca^{2+}, and displayed a good linearity with Ca^{2+} concentration in the range of 2 - 350 μM (Figure 2D). The detection limit was calculated as 220±11 nM (S/N = 3), which can meet the detection requirement in live cells.[34] More importantly, the response time of our developed probe towards Ca^{2+} was less than 2 s (Figure S19), revealing fast response dynamics of the developed nanoprobe towards Ca^{2+}. In addition, both of the fluorescence intensities of CuNCs and AF660 from CuNC@AF660 showed no obvious change (< 5.1%) upon illumination of a Xe lamp (90 W) for 2.5 h, indicating long-term photostability of CuNC@AF660 probe. (Figure S20).

It has been reported that both of metal core and surface ligand shell contribute to the fluorescence of metal nanoclusters.[35] Specifically, the surface ligand shell can influence the fluorescence of metal nanoclusters by charge transfer or electron donation from the ligands to clusters core.[36] In the absence of Ca^{2+} ion, UV-vis absorption spectrum of CuNCs shows three well-resolved absorption peaks at 284, 350 and 476 nm (Figure 1D), which may be due to interband electronic transitions of the Cu clusters from discrete energy levels.[33] The fluorescence of CuNCs show typical emission peak around 590 nm. However, after addition of Ca^{2+}, UV-vis absorption spectra of CuNCs increased while the fluorescence of CuNCs enhanced (Figure S21A, B). Meanwhile, the fluorescence lifetime of CuNCs prolonged from 0.83 ns [7.615 ns (4%); 0.543 ns (96%)] to 6.47 ns (100%) after addition of 400 μM Ca^{2+} (Figure S21C). In order to evaluate the mechanism of fluorescence enhancement of CuNCs, dimethyl sulfoxide (DMSO) was first added in the solution. Since DMSO is hydrogen-bond-breaking polar solvents,[37] the entanglements between the polymer chains can be broken due to the weakening or absence of the hydrogen-bond effect in DMSO. With the increase of the volume fraction of DMSO in the mixed blank solvent ($f = Vol_{DMSO} / Vol_{DMSO+water}$), the fluorescence intensity of CuNCs gradually increased (Figure S22A, B). The fluorescence quantum yield of CuNCs in DMSO (f = 1) increased to 30.7% (Figure S22C), much higher than that (~20%) in water solution. Meanwhile, dynamic light scattering (DLS) results demonstrated that the hydrodynamic diameter of CuNCs in DMSO (f = 1) obviously decreased from98±12 nm (f = 0) to 20±11 nm (Figure S22D). Thus, the fluorescent enhancement of CuNCs was considered to be ascribed to aggregation induced emission because Ca^{2+}-induced aggregation of CuNCs through carboxyl groups in the polymer chain on CuNCs core, leading to the extension of conjugation and increase in the rigidity of the molecular conformation through space electronic interactions, namely, overlap of π and lone pair (n) electrons among carboxyl groups on the polymer.[37]

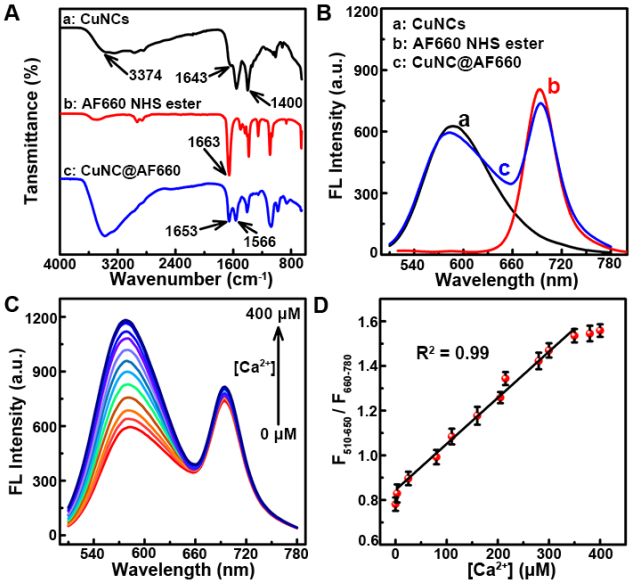

Figure 2. (A) FTIR spectra of CuNCs (a), AF660 NHS ester (b) and CuNC@AF660 (c). (B) Fluorescence spectra of CuNCs (a), AF660 NHS ester (b) and CuNC@AF660 probe (c). (C) Fluorescence responses of CuNC@AF660 (90 μg/mL) with the addition of various concentrations of Ca^{2+} (0, 2, 25, 80, 110, 160, 205, 215, 280, 300, 350, 380, 400 μM) in cell lysis buffer. (D) Calibration curve between $F_{510\text{-}650}/F_{660\text{-}780}$ and various concentrations of Ca^{2+}. Data were obtained from Figure 2C.

Actually, during imaging and biosensing of Ca^{2+} in live cells, not only the sensitivity and detection linearity range but selectivity is also extremely important during analytical processes. Thus, the effect of intracellular potential interferences on the developed sensing probe was studied. The common potential interferences, such as metal ions, physiological relevant amino acids, calcium-containing proteins as well as typical ROS were investigated. In the selectivity test (Figure S23), negligible interferences (< 5.1%) were observed from other metal ions like Mg^{2+} (10 mM), K^+ (100 mM), Na^+ (50 mM), Cu^{2+}, Fe^{2+}, Fe^{3+}, Pb^{2+}, Zn^{2+}, Ag^+, Cd^{2+}, Cr^{3+}, Ni^{2+}, amino acids, calcium-containing proteins like troponin, calpain, and ROS including H_2O_2, $O_2^{\bullet-}$, NO, ROO•, ClO_4^- and •OH. Furthermore, negligible influence (< 4.2%) was observed determination of Ca^{2+} followed by addition of other metal ions, amino acids, calcium-containing proteins and ROS, indicating the high selectively for Ca^{2+} determination against other metal ions, amino acids, calcium-containing proteins and ROS.

Imaging and biosensing of Ca^{2+} in neurons. Before imaging and biosensing of Ca^{2+} in neurons, cytotoxicity and biocompatibility of the developed nanoprobe were in advance evaluated. Cell viability was higher than 90% even at nanoprobe concentration up to 270 μg/mL (Figure S24), which is 3 times as that used in cell imaging. In addition, flow cytometry experimental results showed that no significant increase of apoptotic cells was observed after the neurons were incubated with different concentrations of CuNC@AF660 probe (Figure S25). All these results indicate low cytotoxicity and good biocompatibility of our developed nanoprobe. Moreover, co-localization experimental results demonstrated that the fluorescence of the nanoprobe merged well with that of commercial cytoplasmic probe (CellTracker Green CMFDA), and the Pearson's coefficient was calculated as 0.91 (Figure S26A). It should be pointed out that a small neuronal nucleus was observed in this imaging

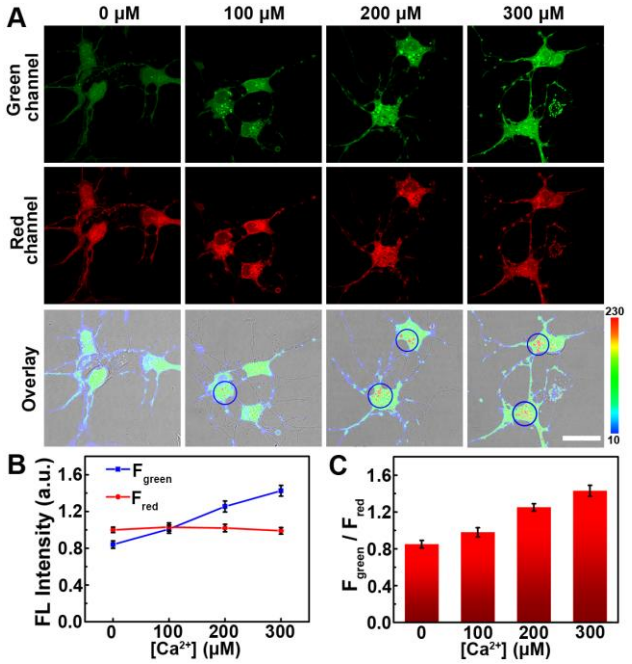

Figure 3. (A) Confocal fluorescence microscopy images of neurons collected from different channels after the neurons were co-incubated with CuNC@AF660 probe (90 μg/mL) in the presence of different concentration of Ca^{2+} (0, 100, 200 and 300 μM), respectively. (B) Average fluorescence intensities of green channel (F_{green}) and red channel (F_{red}) at different concentrations of Ca^{2+}. F_{green} and F_{red} represent the average fluorescence intensity collected from green channel (510-650 nm) and red channel (660-780 nm), respectively. (C) F_{green}/F_{red} values verse different concentration of Ca^{2+}. $F_{green} = F_{510\text{-}650}$, $F_{red} = F_{660\text{-}780}$. Scale = 25 μm.

plane (Z_1 position) (Figure S26A), which is due to specific cell morphology of neurons.[38] Generally, the neuronal nucleus is located in soma of cortical neurons with diameter of 3-18 μm. Meanwhile, the diameter of soma is 30-150 μm. Because the diameters of dendrite and distal axon(0.5~2 μm) are much smaller than those of the soma and neuronal nucleus, the soma and neuronal nucleus are hard to be observed in the same imaging planes as those of dendrite and distal axon. To obtain the distribution of cytoplasm in soma, dendrite, and distal axon simultaneously, the suitable imaging plane (Z_1 position) was chosen during imaging. In this context, neuronal nucleus can hardly be observed in this imaging plane (Z_1 position). However, when the Z_2 position was chosen as imaging plane (Figure S26B), the neuronal nucleus was clearly observed, but the dendrite and distal axon of neuron can hardly be observed. The fluorescence of the present nanoprobe also merged well with that of CellTracker CMFDA in this imaging plane (Z_2 position) and the Person's correlation coefficient was calculated as 0.92. However, the fluorescence of nanoprobe seldom merged with that of 4',6-diamidino-2-phenylindole (DAPI), and the Person's correlation coefficient was calculated as 0.15. All the results demonstrated that the developed CuNC@AF660 probe entered into cells and primary located in cytoplasm.

Then, this nanoprobe was applied for Ca^{2+} sensing and imaging in cytoplasm of neurons. As shown in Figure 3A, with increasing concentration of Ca^{2+} from 0 to 300 μM, green channel became brighter while red channel kept unchanged, demonstrating the fluorescence intensity of F_{green} ($F_{green} = F_{510\text{-}650}$) increased while F_{red} ($F_{red} = F_{660\text{-}780}$) kept stable (Figure 3B). From the merged channel we can see that the pseudo color of neurons

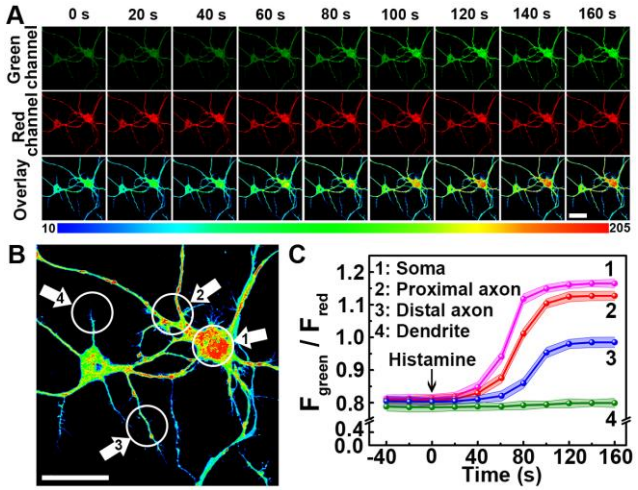

Figure 4. (A) Time-tracking of confocal fluorescence microscopic images of neurons were stimulated by 50 μM histamine for different times. (B) The enlarged image of neurons stimulated by histamine for 160 s. The different zones (1-4) represent the soma, proximal axon, distal axon and dendrite of neuron, respectively. (C) F_{green}/F_{red} value of different zones in neurons after the neurons were stimulated by 50 μM histamine for different times. F_{green} and F_{red} represent the average fluorescence intensity collected from green channel (510-650 nm) and red channel (660-780 nm), respectively. The excitation wavelength was 488 nm. $F_{green} = F_{510\text{-}650}$, $F_{red} = F_{660\text{-}780}$. Scale bars = 25 μm.

changed from blue to red, suggesting our probe can be used for intracellular Ca^{2+} detection. The average fluorescence intensity ratio of green channel to red channel (F_{green}/F_{red}) increased from 0.85 to 1.44 (Figure 3C). It should be noted that there were many bright domains (inside the blue circles) in cytoplasm, which belongs to the Ca^{2+}-rich domains in neurons, suggests the distribution of cytoplasmic Ca^{2+} was inhomogeneous.

More interestingly, it has been reported that histamine can mobilize intracellular Ca^{2+} stores and arise Ca^{2+} levels in live cells. Then, the concentration change of Ca^{2+} was investigated using our developed CuNC@AF660 probe in neurons stimulated by histamine. As shown in Figure 4A, after the neurons were stimulated by 50 μM histamine for 40 s, green channel turned into brighter while red channel kept unchanged. Subsequently, the fluorescence intensity of green channel was continuously enhanced and remained stability after the neurons were stimulated by histamine for 120 s. Interestingly, it was found that histamine-induced Ca^{2+} increase of fluorescent ratio in different regions of neuron was diverse (Figure 4B). As shown in Figure 4C, before the neurons were stimulated by histamine, F_{green}/F_{red} values were basically the same in different regions of the neuron (~0.79±0.04). After the neurons were stimulated by histamine for 120 s, F_{green}/F_{red} values in soma and proximal axon were 1.16±0.05 and 1.12±0.03, respectively. Meanwhile, F_{green}/F_{red} value in distal axon was 0.98±0.04. These results suggested that histamine-induced Ca^{2+} concentration increase was similar in soma and proximal axon, and the increased Ca^{2+} concentration in distal axon of neurons was much lower than that in soma. Unexpectedly, F_{green}/F_{red} value in dendrite of neurons was 0.80±0.05 after the neurons were stimulated by histamine for 120 s, implying that histamine stimulation had no obvious effect on Ca^{2+} concentration in dendrite.

Real-time monitoring of Ca^{2+} level induced by superoxide anion ($O_2^{\bullet-}$). Increasing evidence has indicated that homeo-

static and physiological ROS levels are indispensable in regulating Ca^{2+} burst production, leading to increase in oxidative stress or even cell death,[39] which may be strongly related to many diseases, like cardiovascular diseases and neurodegenerative diseases.[40] $O_2^{\bullet-}$ as the primary species of ROS and precursor of other ROS, has highly oxidative activity.[21,24,41] Excessive accumulation of $O_2^{\bullet-}$ in cells can cause oxidative damage to proteins, DNA, liposomes, and even cell death.[42,43] Based on the established fluorescent CuNC@AF660 probe as a selective and accurate probe for imaging and biosensing of intracellular Ca^{2+}, the effect of $O_2^{\bullet-}$ on cellular Ca^{2+} during stimulation was investigated. The influence of $O_2^{\bullet-}$ on neuronal viability was first evaluated. Neuronal viability obviously decreased with increasing concentration of $O_2^{\bullet-}$ as well as extension of stimulation time (Figure 5A). Higher concentrations of $O_2^{\bullet-}$ resulted in reduced cell viability. It is well-known that, under normal physiological conditions, $O_2^{\bullet-}$ undergoes disproportionation by non-catalytic and enzymatic reactions, resulting in a rather low physiological concentration (10^{-8}-10^{-7} M).[44] Increases in the activity of $O_2^{\bullet-}$ occur in response to traumatic brain injury ischemia-reperfusion, hypoxia, and environmental stresses, the concentration of $O_2^{\bullet-}$ may increase to ~10^{-4} M.[39,41,45,46] As shown in Figure 5A, neuron viability was only ~15±5% after the neurons stimulated by 80 μM $O_2^{\bullet-}$ for 15 h. In order to understand the mechanism of $O_2^{\bullet-}$-induced neuronal death, we then real-time monitored the cytoplasmic Ca^{2+} changes when the neurons were stimulated by 80 μM $O_2^{\bullet-}$. As shown in Figure 5B, F_{green}/F_{red} value clearly increased after the neurons were stimulated by $O_2^{\bullet-}$ for 240 s, and F_{green}/F_{red} value increased from 0.81±0.02 to 1.36±0.04 after the neurons were stimulated by $O_2^{\bullet-}$ for 360 s. According to the established calibration curve in cell lysis (Figure 2C), cytoplasmic Ca^{2+} increased to ~250 μM after the neurons were stimulated by $O_2^{\bullet-}$ for 360 s. It should be pointed out that normal concentration of Ca^{2+} in cytoplasm was about 0.2 μM.[47] These results strongly indicated that $O_2^{\bullet-}$-induced Ca^{2+} burst in neurons. Consistently, the green channel became significantly brighter after the neurons were stimulated by 80 μM $O_2^{\bullet-}$ while the red channel kept no obvious change (Figure 5C). This $O_2^{\bullet-}$-induced cytoplasmic Ca^{2+} burst suggested that $O_2^{\bullet-}$-induced neuronal death was possibly resulted from Ca^{2+} overload in neurons, which may cause Ca^{2+} disorders in neurons and unfavorable for neuron viability.

CONCLUSIONS

In summary, a CuNCs-based ratiometric fluorescent nanoprobe has been developed for real-time biosensing and bioimaging of cytoplasmic Ca^{2+} in neurons, in which a specific CaL was synthesized and conjugated to PEI to prepare PEI-CaL. PEI-CaL plays not only as a recognition element for Ca^{2+}, but also as a new ligand molecular for synthesis of fluorescent CuNCs. Furthermore, AF660 was attached onto the surface of CuNCs to act as a reference element, resulting in a built-in correction to improve the accuracy. This inorganic-organic ratiometric fluorescent nanoprobe has demonstrated long-term stability, as well as high selectivity against other metal ions, amino acids, calcium-containing proteins and ROS. Accordingly, the developed fluorescent nanoprobe with low cytotoxicity and good biocompatibility has been successfully applied in multicolor imaging and biosensing of cytoplasmic Ca^{2+} in neurons. Taking advantages of rapid response dynamics of our developed probe, it has been found that Ca^{2+} in cytoplasm was inhomogeneous. Besides, histamine-induced Ca^{2+} increase in proximal axon of neurons was found to be similar with that in soma. Meanwhile, Ca^{2+} change in neuronal distal axon was less than that in soma, and Ca^{2+} concentration in dendrite had no obvious change after the neurons were stimulated by histamine. More importantly, we have found that $O_2^{\bullet-}$-induced neuronal death might be resulted from the Ca^{2+} overload in neurons, providing a new point of view to understand the mechanism of oxidative stress-related diseases. This study has provided a methodology to develop metal cluster-based inorganic-organic fluorescent probes for metal ions, ROS, and other biological species in neurons.

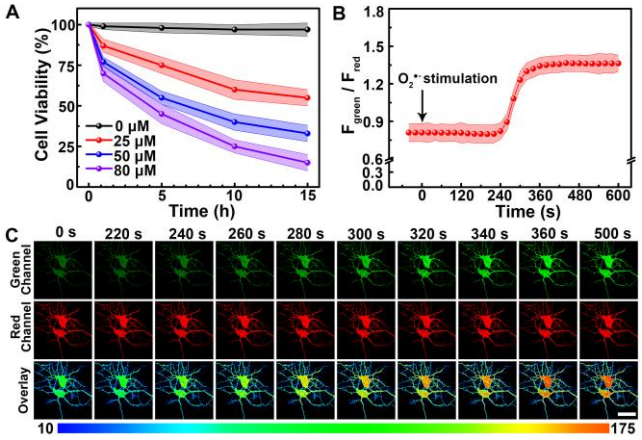

Figure 5. (A) Summarized data of neuron viability after the neurons were stimulated by various concentrations of $O_2^{\bullet-}$ (0, 25, 50 and 80 μM) for different times (0, 1, 5 and 15 h). (B) Time-tracking of F_{green}/F_{red} values obtained every 20 s after the neurons were stimulated by 80 μM $O_2^{\bullet-}$. (C) The typical confocal fluorescence microscopic images of neurons collected from different channels after the neurons were stimulated by 80 μM $O_2^{\bullet-}$ for different times. F_{green} and F_{red} represent the average fluorescence intensity collected from green channel (510-650 nm) and red channel (660-780 nm), respectively. The excitation wavelength was 488 nm. F_{green} = $F_{510\text{-}650}$, F_{red} = $F_{660\text{-}780}$. Scale = 25 μm.

ASSOCIATED CONTENT

Supporting Information

The Supporting Information is available free of charge on the ACS Publications website. Characterization of compound 1, compound 2, compound 3, CaL ester and CaL; Fluorescence quantum yield, XPS spectra and stability investigation of CuNCs. Fluorescence enhancement mechanism research. Selectivity, cytotoxicity and biocompatibility study of CuNC@AF660 probe. Co-localization imaging results.

AUTHOR INFORMATION

Corresponding Author

*Phone + 86 21 54341041; fax +86 21 54341041; E-mail: ytian@chem.ecnu.edu.cn.

ORCID

Yang Tian: 0000-0001-8850-0349

Notes

The authors declare no competing financial interest.

ACKNOWLEDGMENT

The authors greatly appreciate the financial support from NSFC (21635003 and 21827814) and The Program of Shanghai Subject Chief Scientist (15XD1501600). This work also was supported by

Innovation Program of Shanghai Municipal Education Commission (201701070005E00020).

REFERENCES

(1) Clapham, D. E. *Cell* **2007**, *131*, 1047-1058.
(2) Berridge, M. J. *Nature* **1993**, *361*, 315-325.
(3) Plattner, H.; Verkhratsky, A. *Cell Calcium* **2015**, *57*, 123-132.
(4) Barnham, K. J.; Masters, C. L.; Bush, A. I. *Nat. Rev. Drug Discovery* **2004**, *3*, 205-214.
(5) LaFerla, F. M. *Nat. Rev. Neurosci.* **2002**, *3*, 862-872.
(6) Wan, Q.; Chen, S.; Shi, W.; Li, L.; Ma, H. *Angew. Chem. Int. Ed.* **2014**, *53*, 10916-10920.
(7) Kim, S.; Tachikawa, T.; Fujitsuka, M.; Majima, T. *J. Am. Chem. Soc.* **2014**, *136*, 11707-11715.
(8) Setsukinai, K.-i.; Urano, Y.; Kakinuma, K.; Majima, H. J.; Nagano, T. *J. Biol. Chem.* **2003**, *278*, 3170-3175.
(9) Peng, L.; Xu, S.; Zheng, X.; Cheng, X.; Zhang, R.; Liu, J.; Liu, B.; Tong, A. *Anal. Chem.* **2017**, *89*, 3162-3168.
(10) Zhang, W.; Li, P.; Yang, F.; Hu, X.; Sun, C.; Zhang, W.; Chen, D.; Tang, B. *J. Am. Chem. Soc.* **2013**, *135*, 14956-14959.
(11) Miyawaki, A.; Llopis, J.; Heim, R.; McCaffery, J. M. *Nature* **1997**, *388*, 882.
(12) Heim, N.; Griesbeck, O. *J. Biol. Chem.* **2004**, *279*, 14280-14286.
(13) Ohkura, M.; Matsuzaki, M.; Kasai, H.; Imoto, K.; Nakai, J. *Anal. Chem.* **2005**, *77*, 5861-5869.
(14) Tour, O.; Adams, S. R.; Kerr, R. A.; Meijer, R. M.; Sejnowski, T. J.; Tsien, R. W.; Tsien, R. Y. *Nat. Chem. Biol.* **2007**, *3*, 423-431.
(15) Agarwal, H. K.; Janicek, R.; Chi, S.-H.; Perry, J. W.; Niggli, E.; Ellis-Davies, G. C. R. *J. Am. Chem. Soc.* **2016**, *138*, 3687-3693.
(16) Egawa, T.; Hirabayashi, K.; Koide, Y.; Kobayashi, C.; Takahashi, N.; Mineno, T.; Terai, T.; Ueno, T.; Komatsu, T.; Ikegaya, Y.; Matsuki, N.; Nagano, T.; Hanaoka, K. *Angew. Chem. Int. Ed.* **2013**, *52*, 3874-3877.
(17) Mishra, A.; Jiang, Y.; Roberts, S.; Ntziachristos, V.; Westmeyer, G. G. *Anal. Chem.* **2016**, *88*, 10785-10789.
(18) Li, Z.; Lv, S.; Wang, Y.; Chen, S.; Liu, Z. *J. Am. Chem. Soc.* **2015**, *137*, 3421-3427.
(19) Song, X.; Yue, Z.; Zhang, J.; Jiang, Y.; Wang, Z.; Zhang, S. *Chem. Eur. J.* **2018**, *24*, 6458-6463.
(20) Zhu, A.; Qu, Q.; Shao, X.; Kong, B.; Tian, Y. *Angew. Chem. Int. Ed.* **2012**, *51*, 7185-7189.
(21) Gao, X.; Ding, C.; Zhu, A.; Tian, Y. *Anal. Chem.* **2014**, *86*, 7071-7078.
(22) Han, Y.; Ding, C.; Zhou, J.; Tian, Y. *Anal. Chem.* **2015**, *87*, 5333-5339.
(23) Liu, Z.; Wang, S.; Li, W.; Tian, Y. *Anal. Chem.* **2018**, *90*, 2816-2825.
(24) Huang, H.; Dong, F.; Tian, Y. *Anal. Chem.* **2016**, *88*, 12294-12302.
(25) Zhuang, M.; Ding, C.; Zhu, A.; Tian, Y. *Anal. Chem.* **2014**, *86*, 1829-1836.
(26) Shi, W.; Li, X.; Ma, H. *Angew. Chem. Int. Ed.* **2012**, *51*, 6432-6435.
(27) Liu, J.-M.; Chen, J.-T.; Yan, X.-P. *Anal. Chem.* **2013**, *85*, 3238-3245.
(28) Pan, W.; Wang, H.; Yang, L.; Yu, Z.; Li, N.; Tang, B. *Anal. Chem.* **2016**, *88*, 6743-6748.
(29) Li, P.; Fang, L.; Zhou, H.; Zhang, W.; Wang, X.; Li, N.; Zhong, H.; Tang, B. *Chem. Eur. J.* **2011**, *17*, 10520-10523.
(30) Grynkiewicz, G.; Poenie, M.; Tsien, R. Y. *J. Biol. Chem.* **1985**, *260*, 3440-3450.
(31) Rama Rao, A. V.; Laxma Reddy, K.; Machender Reddy, M. *Tetrahedron Lett.* **1994**, *35*, 5039-5042.
(32) Liu, Z.-C.; Qi, J.-W.; Hu, C.; Zhang, L.; Song, W.; Liang, R.-P.; Qiu, J.-D. *Anal. Chim. Acta* **2015**, *895*, 95-103.
(33) Wei, W.; Lu, Y.; Chen, W.; Chen, S. *J. Am. Chem. Soc.* **2011**, *133*, 2060-2063.
(34) Montero, M.; Alonso, M. T.; Carnicero, E.; Cuchillo-Ibanez, I.; Albillos, A.; Garcia, A. G.; Garcia-Sancho, J.; Alvarez, J. *Nat. Cell Biol.* **2000**, *2*, 57-61.
(35) Chen, Y.; Yang, T.; Pan, H.; Yuan, Y.; Chen, L.; Liu, M.; Zhang, K.; Zhang, S.; Wu, P.; Xu, J. *J. Am. Chem. Soc.* **2014**, *136*, 1686-1689.
(36) Wu, Z.; Jin, R. *Nano Lett.* **2010**, *10*, 2568-2573.
(37) Yang, T.; Dai, S.; Yang, S.; Chen, L.; Liu, P.; Dong, K.; Zhou, J.; Chen, Y.; Pan, H.; Zhang, S. *J. Phys. Chem. Lett.* **2017**, *8*, 3980-3985.
(38) Liu, Z.; Pei, H.; Zhang, L.; Tian, Y. *ACS Nano* **2018**, *12*, 12357-12368.
(39) Wang, W.; Fang, H.; Groom, L.; Cheng, A.; Zhang, W.; Liu, J.; Wang, X.; Li, K.; Han, P.; Zheng, M.; Yin, J.; Wang, W.; Mattson, M. P.; Kao, J. P. Y.; Lakatta, E. G.; Sheu, S.-S.; Ouyang, K.; Chen, J.; Dirksen, R. T.; Cheng, H. *Cell* **2008**, *134*, 279-290.
(40) Li, P.; Zhang, W.; Li, K.; Liu, X.; Xiao, H.; Zhang, W.; Tang, B. *Anal. Chem.* **2013**, *85*, 9877-9881.
(41) Turrens, J. F. *J. Physiol.* **2003**, *552*, 335-344.
(42) Liou, G.-Y.; Storz, P. *Free. Radical. Res.* **2010**, *44*, 479-496.
(43) Fridovich, I. *Annu. Rev. Biochem.* **1995**, *64*, 97-112.
(44) Cadenas, E.; Davies, K. J. *Free. Radical. Bio. Med* **2000**, *29*, 222-230.
(45) Deng, Z.; Rui, Q.; Yin, X.; Liu, H.; Tian, Y. *Anal. Chem.* **2008**, *80*, 5839-5846.
(46) Gorrini, C.; Harris, I. S.; Mak, T. W. *Nat. Rev. Drug Discovery* **2013**, *12*, 931-947.
(47) Coll, K. E.; Joseph, S.; Corkey, B.; Williamson, J. *J. Biol. Chem.* **1982**, *257*, 8696-8704.

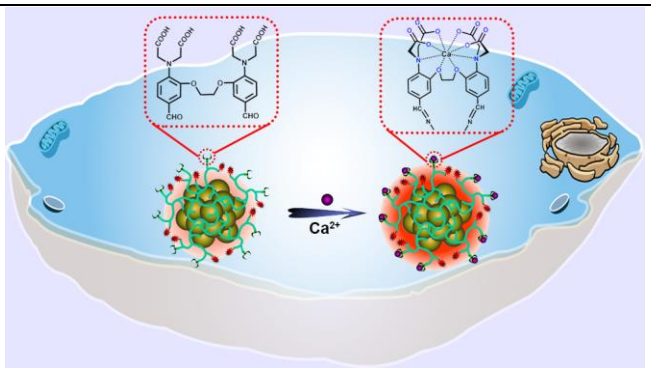

For TOC only